HHS Public Access

Author manuscript

J Neural Eng. Author manuscript; available in PMC 2016 February 01.

Published in final edited form as:

J Neural Eng. 2015 February ; 12(1): 016008. doi:10.1088/1741-2560/12/1/016008.

Evaluation of poly(3,4-ethylenedioxythiophene)/carbon nanotube neural electrode coatings for stimulation in the dorsal root ganglion

Christi L. Kolarcik[a,c,d], **Kasey Catt**[a], **Erika Rost**[a], **Ingrid N. Albrecht**[b], **Dennis Bourbeau**[b,e], **Zhanhong Du**[a,c,d], **Takashi D.Y. Kozai**[a,c,d], **Xiliang Luo**[a,f], **Douglas J. Weber**[a,b], and **X. Tracy Cui**[a,c,d]

[a]Department of Bioengineering, University of Pittsburgh, Pittsburgh, PA USA

[b]Department of Physical Medicine and Rehabilitation, University of Pittsburgh, Pittsburgh, PA USA

[c]Center for the Neural Basis of Cognition, University of Pittsburgh, Pittsburgh, PA USA

[d]McGowan Institute for Regenerative Medicine, University of Pittsburgh, Pittsburgh, PA USA

[e]Department of Veterans Affairs, Case Western Reserve University, Cleveland, OH USA

[f]Key Laboratory of Biochemical Analysis, Ministry of Education, College of Chemistry and Molecular Engineering, Qingdao University of Science and Technology, Qingdao 266042, China

Abstract

Objective—The dorsal root ganglion (DRG) is an attractive target for implanting neural electrode arrays that restore sensory function or provide therapy via stimulation. However, penetrating microelectrodes designed for these applications are small and deliver low currents. For long-term performance of microstimulation devices, novel coating materials are needed in part to decrease impedance values at the electrode-tissue interface and to increase charge storage capacity.

Approach—Conductive polymer poly(3,4-ethylenedioxythiophene) (PEDOT) and multiwall carbon nanotubes (CNTs) were coated on the electrode surface and doped with the anti-inflammatory drug, dexamethasone. Electrode characteristics and the tissue reaction around neural electrodes as the result of stimulation, coating and drug release were characterized. Hematoxylin and eosin staining along with antibodies recognizing Iba1 (microglia/macrophages), NF200 (neuronal axons), NeuN (neurons), vimentin (fibroblasts), caspase-3 (cell death) and L1 (neural cell adhesion molecule) were used. Quantitative image analyses were performed using MATLAB.

Main Results—Our results indicate that coated microelectrodes have lower *in vitro* and *in vivo* impedance values. Significantly less neuronal death/damage was observed with coated electrodes as compared to non-coated controls. The inflammatory response with the PEDOT/CNT-coated electrodes was also reduced.

Corresponding author: X. Tracy Cui, Ph.D., Department of Bioengineering, University of Pittsburgh, 5057 Biomedical Science Tower 3, 3501 Fifth Avenue, Pittsburgh, PA 15260, Ph: 412-383-6672, FAX: 412-383-5918, xic11@pitt.edu.

Significance—This study is the first to report on the utility of these coatings in stimulation applications. Our results indicate PEDOT/CNT coatings may be valuable additions to implantable electrodes used as therapeutic modalities.

Keywords

tissue/electrode interface; neural probes; DRG; PEDOT/CNT; dexamethasone; microstimulation

1. Introduction

Electrical stimulation of electrically responsive tissues (i.e., brain, heart, skeletal muscle) has been investigated for a variety of applications including vagal nerve stimulation, retinal and cochlear implants, spinal cord stimulation and deep brain stimulation [1]. In most of these applications, electrodes are relatively large and the current delivered relatively high (hundreds of μA to mA). In contrast, penetrating microelectrodes designed for microstimulation are comparatively small, deliver much lower currents and enable better spatial resolution of the electrical stimulus. In the nervous system, spatial specificity is particularly important as discrete and graded sensations can be evoked through stimulation [2-6]. However, even minor tissue damage and scarring can compromise resolution at the microelectrode-tissue interface. In addition, the charge densities for microelectrodes are high and electrode degradation is of concern [7].

In the clinical setting, effective activation of neurons must be achieved while the extent of tissue injury minimized. Proper management of this trade-off between target activation and tissue injury/electrode degradation is critical for maintaining long-term, functional contact with the neural tissue surrounding the electrode. However, it is only one of the factors contributing to stimulation electrode failure. Biocompatibility issues resulting in immune and inflammatory reactions prevent functional integration with the surrounding neural tissue and cause chronic neuronal degeneration [8, 9]. These tissue responses negatively affect electrode performance and are often referred to as biotic effects (reviewed in [10]). However, abiotic effects (i.e., physical changes to the electrode) impact electrical properties as well [10]. In the complex and dynamic environment surrounding the electrode, a combination of these factors can lead to a detrimental cascade of events. These include extensive scar tissue that can decrease the density of neurons at the electrode-tissue interface and the formation of a high impedance layer that minimizes signal transduction both from and to the tissue. Higher impedance requires higher current to elicit an equivalent response resulting in greater power consumption, more damage to the electrode and surrounding tissue and ultimately, decreased electrode performance.

Indeed, many research groups are exploring ways to overcome these technical challenges. For example, high voltage pulses to disrupt scar tissue [11, 12] and localized delivery of anti-inflammatory drugs and neurotrophic factors [13-17] have been investigated. To address the mechanical mismatch between current electrode materials and brain tissue, a number of groups are also investigating soft materials with mechanical properties similar to those of central nervous system (CNS) or peripheral nervous system (PNS) tissue [18-23]. Despite the tissue integration and functionality demonstrated with ultrasmall electrodes [24,

25], there has yet to be a technique that successfully mitigates the biotic and abiotic effects that result in poor chronic electrode performance. In addition, it is difficult to achieve high charge delivery capacity with microelectrodes.

One approach used by our laboratory and others involves modification of electrodes with conducting polymers. These biocompatible and inherently conductive polymers are an attractive material for neural stimulation applications. They exhibit both fast and high charge delivery capacities as a result of the high ionic conductivity and large electroactive surface area [26] resulting in low impedance and more effective charge transfer [27]. Among the various conducting polymers, poly(3,4-ethylenedioxythiophene) (PEDOT) has been shown to be an excellent material for neural stimulation as a result of its superior impedance and charge injection capacity when compared to thin film platinum (Pt) electrodes [7, 28, 29]. Furthermore, PEDOT has improved electrochemical, mechanical and thermal stability necessary for use in chronic implants [30]. However, delamination of thick PEDOT films has been observed with prolonged stimulation and is affected by underlying electrode surface roughness as well as the dopant molecule [31]. Additionally, anti-inflammatory agents like dexamethasone have been successfully incorporated and electrically released from conducting polymers to inhibit the inflammatory tissue response [27, 32]. However, the drug-loading capacity of PEDOT alone is limited, the amount of drug released during stimulation cycles is not consistent or sustainable and the electrical properties of drug-doped films are suboptimal. These factors highlight a need for improved PEDOT coatings to enable sufficient and reproducible drug release and to improve upon electrical properties.

To address these limitations, carbon nanotube (CNT) doped polymers have recently been developed. CNT/conducting polymer composites have better conductivity when compared to PEDOT films doped with polystyrene sulfonate (PSS), and PEDOT/CNT films demonstrated improved stability (i.e., no delamination or cracking) even after prolonged and aggressive stimulation [33-35]. In addition, CNTs have low toxicity, no immunogenicity [36-38] and can act as a nanoreservoir for targeted drug delivery using controlled drug release [39, 40]. For example, multiwall CNTs loaded with dexamethasone were able to reduce the extent of microglial activation in response to lipopolysaccharide treatment to a similar extent as an exogenously administered drug [41]. The combination of PEDOT, CNTs and dexamethasone takes advantage of the increased conductivity of CNT dopant and improves upon the capacity to effectively store drug molecules and then release the bioactive drug in a controlled manner using electrical stimulation.

The purpose of this study was to evaluate the effects of stimulation in the rat dorsal root ganglion (DRG) on electrode impedance characteristics and tissue response. We then compared the effects of three different coating conditions: non-coated (NC), PEDOT/CNT coated (PC) and PEDOT/CNT/Dexamethasone coated (PCD). The stimulation paradigm was designed to activate sensory neurons in the DRG based on previous acute studies [2]. These values were also consistent with those used by McCreery and colleagues [42] with a rationale for these parameters established in work by Schmidt and colleagues [43, 44]. The results indicate that stimulation results in lower impedance (Z) values and that both PC and PCD coatings are associated with lower Z at specific time points when compared to NC

electrodes. Furthermore, decreases in axonal damage and neuronal cell death are observed with the PC- and PCD-coated electrodes relative to the NC electrodes.

2. Methods

2.1. Dual electrode fabrication

Dual-shank microelectrodes were custom built using a pair of platinum/iridium electrodes (MicroProbes, Gaithersburg, MD) cut to a length of approximately 2.5 mm with an inter-shank spacing of 100-700 μm. Nichrome wires (Formvar-insulated, approximately 3-4 mm in length) were used to form an intermediate connection between the microelectrodes and the percutaneous lead wires. Lead wires were constructed with Teflon-insulated multi-stranded stainless steel wire (AS-631, Cooner Wire Company, Chatsworth, CA). A micro-welder was used to bond the lead junction. These lead wires were routed subdurally to a connection affixed to the skull (overall design depicted in Figure 1). The welded joints were covered with light-curing dental cement and then insulated with a layer of Kwik-Sil (WPI, Inc., Sarasota, FL). Prior to implantation, electrodes were tested, cleaned and sterilized using ethylene oxide (EtO).

2.2. Coating procedure

All multi-wall carbon nanotubes (CNTs) used for electrode coatings were first functionalized using strong acid treatment. Treatment consisted of mixing 200 mg of CNTs (outer diameter 20-30 nm, inner diameter 5-10 nm, length 10-30 μm, purity >95%; Cheap Tubes, Inc., Brattleboro, VT) with 100 mL of 1:3 concentrated HNO_3 (Sigma, St. Louis, MO) and H_2SO_4 (Sigma) via sonication for 2 hours. This solution was then stirred at room temperature overnight. Acid was removed by rinsing the CNT solution with sterile water using an ultracentrifuge. Rinsing was stopped when the solution reached neutral pH and the tubes collected and dried at 60°C.

Both PEDOT/CNT (PC) and PEDOT/CNT/Dexamethasone (PCD) coatings were polymerized under sterile conditions using a Gamry Potentiostat, FAS2/Femtostat (Gamry Instruments, Warminster, PA) with Gamry Framework software. A conventional three-electrode system with the platinum (Pt) microelectrode or dual microelectrode acting as the working electrode, a Pt wire as the counter electrode and a silver/silver chloride (Ag/AgCl) wire as the reference electrode (CH Instruments, Austin, TX) was used. Prior to coating, probes were electrochemically pretreated in phosphate buffered saline (PBS; pH 7.4) at −2V for 20s. For the PC coating, electropolymerization was carried out in an aqueous solution of 0.02 M 3,4-ethylenedioxythiophene (EDOT; Sigma) containing 1 mg/mL CNT with a constant current of 40 nA applied for 5s as described previously [33]. For the PCD coating, an aqueous solution containing 20 mg/mL dexamethasone 21-phosphate disodium salt (Sigma) and 1 mg/mL CNTs was first sonicated for one hour to facilitate drug loading into the tubes. After sonication, PEDOT was added to a concentration of 0.02 M and polymerized at 1.4V for 30s for the first shank followed by constant current polymerization for 30s on the second shank as described previously [41]. Average current and current density were 12.4 μA and 372 $\mu C/\mu m^2$, respectively. Electropolymerization of PCD electrodes was carried out in an aqueous solution containing dexamethasone-loaded CNTs

as well as free dexamethasone (not loaded into the CNTs). Therefore, PCD coatings are doped by both the dexamethasone-filled CNTs as well as the free dexamethasone.

2.3. Electrochemical impedance spectroscopy

The electrochemical impedance spectroscopy (EIS) was measured with the Gamry Potentiostat, FAS2/Femtostat (Gamry Instruments) with Gamry Framework software using a three-electrode system. The EIS was measured in PBS in the frequency range from 0.5 Hz to 100 kHz using an alternating current sinusoid of 5 mV in amplitude with the direct current potential set to 0 V and recorded at 10 points/decade.

2.4. In vitro drug release

To quantify the amount of dexamethasone released with the stimulation parameters outlined above, PEDOT/CNT/Dexamethasone coatings were deposited onto reusable 3 mm diameter glassy carbon (GC) electrodes (CH Instruments, Austin, TX). First, GC surfaces were electrochemically treated with 1.8 V for 250 s followed by 5 cycles of cyclic voltammetry from 0.3 to 1.3 V at a scan rate of 100 mV/s in PBS using the three-electrode system described above. Polymerization of PEDOT/CNT/Dexamethasone was carried out in the same solution as that used for the microwires using a constant current of 70 μA for 150 s. These electrodes were then stimulated using a two-electrode system with a Pt sheet acting as the reference and counter. The hour long stimulation protocol consisted of −1.48 V for 200 μs followed by 0.74 V for 400 μs and was applied to each electrode at a frequency of 200 Hz. This protocol mimicked the average voltage excursion observed with the PCD coating *in vivo* on the day of implant. The amount of dexamethasone release was calculated per stimulation cycle. To quantify dexamethasone release, solutions with released drug were transferred to a half area 96-well ultraviolet (UV) transparent Costar 4679 assay plate and UV absorption measured using the Spectramax M5 (Molecular Devices, Sunnyvale, CA) at 242 nm.

2.5. Surgical procedure

All surgical procedures were done in accordance with those outlined by the United States Department of Agriculture and approved by the Institutional Animal Care and Use Committee of the University of Pittsburgh. Animals were housed in the facilities of the University of Pittsburgh Department of Laboratory Animal Resources and given free access to food and water.

Fourteen adult male Sprague-Dawley rats (300 ± 50 g) were used throughout this study. For each stimulation group, three animals were implanted in the dorsal root ganglion (DRG) with electrodes with no coating, PEDOT/CNT coating or PEDOT/CNT/Dexamethasone coating. Unstimulated controls (1-2 animals/coating) were also included (outlined in Table 1).

Animals were anesthetized with 2.5% isofluorane in 0.8 L/min oxygen for 5 minutes prior to surgery and then maintained for the duration of the procedure with 1-2% isofluorane. Anesthesia level was monitored closely during the procedure by observing changes in respiratory rate, heart rate, expired CO_2, body temperature (37.7°C) and absence of the

pedal reflex. Ophthalmic ointment was applied to the eyes while animals were under anesthesia.

Animals were placed in a stereotaxic frame and the hair removed over the incision sites (head and back). The skin was disinfected with isopropyl alcohol and betadine surgical scrub solution and a sterile environment maintained throughout the procedure. One incision was made along the spinal column, the skin retracted and the fascia and tissue cleared/removed to expose the caudal portion of the vertebral column. A unilateral laminectomy was performed to expose the left side of the DRG between L5 and L6. Every attempt was made to minimize removal and/or cutting of muscle and bone surrounding the area of implant. Once exposed, dual microelectrodes were inserted using a micromanipulator equipped with a vacuum; microelectrodes were held in place with the vacuum, positioned by moving the micromanipulator and then lowered into place. Leads were run up the back of the animal, and a second incision was made along the scalp and the skin retracted to expose the skull. Bone screws were hand-drilled and ground wires (Cooner wire) wrapped around two of the three screws. Connectors to the implanted electrodes were fixed on the skull with light-curing dental cement and included pins to connect to electrode 1, electrode 2 and the ground. After the muscle and skin were sutured, the animal recovered under close supervision in the surgical procedure room. Rats were monitored closely for signs of pain or distress and post-operative pain managed with buprenorphine (0.3 mg/kg). The same surgical team performed all surgeries to minimize variability associated with the surgery and electrode implantation.

2.6. Stimulation protocol

The stimulation regimen was initiated 3 days after electrode implantation to allow for recovery. For each dual electrode, the coating condition and stimulation group were kept the same. In stimulation groups, the electrodes were pulsed for 1 h per day on 10 of 14 study days using an RX7 microstimulation system (Tucker-Davis Technologies, Alachua, FL) to deliver biphasic current pulses consisting of a leading 200 μs cathodic pulse followed by a 400 μs anodic phase of half amplitude to maintain charge balance. Ground wires were placed on two of the skull screws and in the epidural space along the spinal cord. The amplitude of the cathodic phase was 20 μAmps, and stimulation pulses were applied at a rate of 200 Hz.

To characterize electrical performance, 1001 stimulus pulse trains were generated at 200 Hz using a potentiostat (Autolab PGSTAT128N, Metrohm USA, Riverview, FL) using a bone screw as a reference. 1000 pulses were used to stabilize the electrode potential from any "ratcheting" effects [45]. On the 1001st stimulus pulse, the steady-state voltage response to the current-controlled stimulus waveform was recorded. The highest positive and the lowest negative potential that the electrode experienced during the stimulation waveform were measured and compared to the impedance. CV measurements were made at 50 mV/s between potential limits of −0.6 V and 0.8 V. These CVs were then used to determine the CSC by calculating the time integral of the negative current during a full CV cycle.

During the 1 h of daily stimulation, animals were sedated with dexemedetomidine hydrochloride (Dexdomitor, 0.105 mg/kg). Maintenance doses were administered as necessary (0.03 mg/kg). Following stimulation, animals were revived with atipamezole

hydrochloride (Antisedan, 0.3 mg/kg) and monitored to ensure normal behavior and for alertness. For all stimulated animals, the stimulus was applied continuously (100% duty cycle) on all channels synchronously.

2.7. Antibodies

Monoclonal antibodies were used to detect neurofilament 200 kD (NF200; Millipore, Billerica, MA), vimentin (Clone V-9; Millipore) and neuronal nuclei (NeuN; Millipore). Polyclonal antibodies were used to detect Iba1 (Wako Chemicals USA, Inc., Richmond, VA), L1 (a kind gift from Dr. Carl Lagenaur) and cleaved caspase-3 (Asp175; Cell Signaling Technology, Boston, MA). These antibodies were used at a dilution of 1:500 (NF200, Iba1, Vimentin, L1, NeuN) or 1:50 (cleaved caspase-3) and the appropriate fluorescence-conjugated antibody used at a dilution of 1:500.

2.8. Tissue preparation and immunofluorescence

Seventeen days after surgery, animals were anesthetized with a ketamine/xylazine cocktail (100/20 mg/kg) via the intraperitoneal (IP) cavity. Animals were then transcardially perfused with cold (4°C) PBS followed by 4% (w/v) paraformaldehyde (PFA) in PBS. The DRG tissue was removed, post-fixed for up to 3 days and then equilibrated in 30% sucrose. Following removal of the implant, dissected tissue was cryoprotected using the optimal cutting temperature (OCT) compound (Tissue-Tek, Torrance, CA). Serial sections were cut at a 10 μm thickness.

To ensure that the interface evaluated corresponded to the conductive tip, serial sections were cut through each block of tissue until the implant site was no longer visualized via microscopy. This was done during sectioning prior to staining and confirmed after sectioning and staining. The sections immediately preceding this section were used for immunohistochemistry. These locations were further compared to sections along the length of the electrode shanks. Explanted dual microelectrodes were carefully examined for tissue remnants and coating integrity using scanning electron microscopy (SEM). Tissue was visible on one explant from each of the three coating conditions; these interfaces were excluded from the quantitative analysis. Examination of coated microelectrodes revealed intact coatings.

Tissue sections were stained at the same time for each antibody/antibody pair to minimize variability. Hematoxylin and eosin (H and E) staining along with markers to visualize mature axons (NF200), microglia (Iba1), astrocytes/fibroblasts/endothelial cells (vimentin), neural adhesion molecule (L1), neuronal nuclei (NeuN) and cell death (cleaved caspase-3) (antibodies outlined in Table 2) were used.

Tissue sections were hydrated in PBS and non-specific binding blocked with 0.5% BSA after which primary antibodies diluted in 0.5% BSA were added for approximately 1 hour. After washing, fluorophore-conjugated secondary antibodies (goat anti-mouse Alexa Fluor 488 and goat anti-rabbit Alexa Fluor 594) diluted in 0.5% BSA were added for approximately 1 hour and Hoechst used as the nuclear stain. Fluoromount-G (Southern Biotechnology Associates, Birmingham, AL) was used for mounting and to preserve

fluorescence. Negative controls lacking primary antibody were included for each secondary antibody.

2.9. Quantitative tissue analysis

Confocal fluorescent microscopy was used to evaluate the cellular reactions associated with the implanted electrodes. Images were acquired using an Olympus Fluoview 1000 I Confocal Microscope (Olympus America, Center Valley, PA) at the Center for Biologic Imaging at the University of Pittsburgh. For each antibody, images were acquired using the same laser intensity and exposure time to reduce variability during data analysis.

For quantification of NF200 and Iba1 staining, custom MATLAB (MathWorks, Natick, MA) scripts were used to perform automated intensity-based analyses of a radial probe. For the size of the kill zone, NF200-stained images were used while Iba1-stained images were analyzed to assess the decline in the inflammatory reaction with distance. The kill zone was identified by the area absent of NF200 staining, and quantification of this area was performed as described previously [46]. For Iba1, the center of the region of interest (ROI) was identified and 10 μm bins analyzed for fluorescence staining. To normalize fluorescence intensities, background noise intensity thresholds were calculated based on the pixel intensity measured in the corners of the image (10% of each of the four corners, > 250 μm away from the implant). Pixels with intensity greater than one standard deviation dimmer than mean pixel intensity were considered “signal” and removed from the calculation. The threshold was then determined by calculating the pixel intensity of one standard deviation below the mean of the remaining pixel intensities. The distance at which the peak Iba1 intensity was observed was calculated and compared. For NeuN/caspase-3 stained images, the number of NeuN/caspase-3 positive cells was quantified and reported as a percentage of total NeuN positive cells.

2.10. Statistical analyses

Statistical analyses were performed using GraphPad Prism 5 (GraphPad Software, Inc., La Jolla, CA). Comparisons between treatment groups were accomplished using two-way analysis of variance (ANOVA) followed by Bonferroni post-hoc analysis unless indicated otherwise. A p value ≤ 0.05 was considered statistically significant.

3. Results

Although the DRG is an attractive site for recording or stimulating primary afferent neurons to provide sensory feedback [2, 47], studies investigating the tissue reaction in response to stimulation are lacking. To further investigate this peripheral site, we implanted dual-shank microelectrodes into adult rats and subjected animals to a daily stimulation regimen over a two-week time period. For these studies, electrodes were implanted into the DRG at either L5 or L6 with lead wires connected to an adaptor on the skull of the animal allowing for repeated stimulation (animals in each group outlined in Table 1). The paradigm utilized was based on that used previously in the cerebral cortex of the cat [42] and an overview of our approach is provided in Figure 1.

3.1. Coating morphology

Following fabrication of the dual microelectrodes, one of two modifications was made to the electrode surface. For the first, acid-pretreated CNTs were doped into the backbone of PEDOT during electropolymerization as described previously [33]. In the resulting PEDOT/CNT (PC) coating, CNTs were well-dispersed and formed a network-like structure (Figure 2B, D) unlike that observed by others [48]. For the second coating, dexamethasone was sonicated with the CNTs prior to combining with the EDOT monomer to facilitate loading of the dexamethasone into the CNTs to produce the PEDOT/CNT/Dexamethasone (PCD) coating (Figure 2C, E). Despite the rough and non-uniform substrate of the uncoated electrodes, both coatings were generally uniform and the surfaces show a nanofibrous morphology that is more porous than the non-coated (NC) controls (Figure 2A).

3.2. In vitro electrical performance

Compared to the NC electrodes, the PC coating was associated with significantly lower *in vitro* impedance across all frequencies while the PCD coatings had intermediate impedance values around and below 1 kHz (Figure 3A). The intermediate impedance of the PCD film can be attributed to the additional doping of the free dexamethasone which has been shown to yield films with less substantial impedance decreases [32, 41]. The phase plots indicated different behaviors for each group as well (Figure 3B). For the NC electrodes, the phase indicates a more capacitive nature at lower frequencies and trends toward a more resistive behavior as the frequency increases. The PC coating showed pure capacitance at low frequencies (<100 Hz) and subsequently became more resistive as the frequency increased. The significantly greater effective surface area with the PC coating results in a higher capacitance such that the dominant impedance barrier is resistive at much lower frequencies than the bare metal electrodes. The differences observed between the PC and PCD electrodes are likely due to the co-doping of the free dexamethasone in the PCD film. The incorporation of free dexamethasone reduces the porosity and conductance of the polymer coating by occupying loci on the polymer backbone that could have been filled by the more electrically beneficial CNTs.

3.3. In vitro drug release

In vitro studies were used to evaluate the amount of dexamethasone released as a function of the number of stimulations. Electrodes were stimulated ten times with the hour long stimulation protocol used *in vivo* and compared to equivalent electrodes allowed to diffuse into solution for the same time period. Both stimulated and unstimulated samples showed a higher average release after the first stimulation of 10.9 μg dexamethasone/cm^2 and 5.4 μg dexamethasone/cm^2, respectively. Following the initial release, an average of 2.3 μg dexamethasone/cm^2 per release and 0.9 μg dexamethasone/cm^2 per release for the stimulated and unstimulated samples was observed. After the ten stimulations, a total of 31.4 ± 4.9 μg dexamethasone/cm^2 was released while diffusion alone resulted in a total of 13.0 ± 1.5 μg dexamethasone/cm^2. Using an instantaneous source diffusion model [49] and a dexamethasone diffusion coefficient in brain tissue [50], the average concentration of dexamethasone was determined within 500 μm of the implant one day post-stimulation. The initial release stimulus resulted in an average concentration of 14.5 μM and the following

releases resulted in an average concentration of 3 μM within 500 μm of the implant one day after release. Prior studies have demonstrated the ability of dexamethasone to reduce the inflammatory reaction around neural implants at concentrations between 0.2 and 0.7 μM [51, 52] indicating that the hour long stimulation of the PCD coated-electrodes yields a biologically significant amount of dexamethasone release over the course of this study. Additionally, *in vitro* data shows the stimulated drug release profile does not exhibit a plateau during the ten applied releases suggesting that drug remains available for release. It should be noted that this is a theoretical estimate based on brain tissue; diffusion in the DRG would differ from that in the brain but this value has not been established. Moreover, greater variability among electrode sites would be expected as a result of the heterogeneity of the DRG (i.e., electrodes placed near cell bodies versus those near axons).

3.4. In vivo electrode performance

For the *in vivo* studies, a number of measures were taken for both non-stimulated and stimulated electrodes. First, the effect of stimulation on the impedance (Z) value at 1 kHz was determined. With stimulation, there was a significant decrease in the 1 kHz Z for all coated and uncoated electrodes (103.3 ± 2.7 versus 64.8 ± 2.2 kOhms; Figure 4A; $p < 0.001$). The potential changes in Z over time by coating condition were then evaluated. Without stimulation, there were no significant differences in Z between the three coating conditions (Figure 4B). In addition, there were no statistically significant changes in Z without stimulation for any of the coating conditions (data not shown). However, with stimulation, the Z for PC-coated (Figure 4C; $p < 0.05$ for days 1-3, 65.3 ± 6.8 kOhms) and PCD-coated electrodes (Figure 4C; $p < 0.05$ for days 1-3, 58.4 ± 7.3 kOhms and days 4-7, 53.9 ± 4.2 kOhms) were significantly lower than the Z for NC electrodes (days 1-3, 86.5 ± 6.9 kOhms and days 4-7, 77.7 ± 5.3 kOhms). The more prolonged lowering of the Z for the PCD-coating may be a result of the repeated release of dexamethasone which could reduce tissue inflammation and indirectly influence Z values.

The correlation between Z and maximum electrode potential (both the highest positive and lowest negative potential that the electrode experienced during stimulation) was then evaluated to ensure that our stimulation and Z measures were valid (Figure 4D). The results of Pearson correlation tests indicate that Z values correlate with both + potential ($p < 0.001$; $R^2 = 0.4323$) and – potential ($p < 0.001$; $R^2 = 0.5604$). This correlation underscores the benefit of lower Z values. That is, lower electrode potentials are safer for both the tissue and the implanted electrode.

Finally, cyclic voltammetry (CV) measures were obtained and compared across coating conditions *in vivo* (Figure 5). Representative CV responses for each of the three coating conditions at 1-3 days, 4-7 days and 8-10 days *in vivo* are provided.

3.5. Tissue response

A number of histological stains were performed to characterize the tissue reaction in response to the NC, PC-coated and PCD-coated electrodes (antibodies outlined in Table 2). First, to determine the degree of neuronal and axonal loss around the implant site, NF200 was used. NF200 staining was decreased or absent in the area immediately surrounding the

implant site (Figure 6A). MATLAB was used to quantify and compare the size of this kill zone. Significant increases in kill zone size were observed for NC electrodes (119.1 ± 42.2 μm) when compared to either PC-coated (64.7 ± 32.1 μm; Figure 6B; $p < 0.001$) or PCD-coated (66.4 ± 25.5 μm; Figure 6B; $p < 0.001$) electrodes (values reported are mean ± SD).

We also sought to characterize some of the non-neuronal cellular response including the reactions associated with microglia/macrophages and fibroblasts using Iba1 and vimentin antibodies, respectively. Cells that stained positive for Iba1 were localized to the area immediately surrounding the implant; the staining intensity was highest at or near the site of the implant and decreased further from this interface (Figure 6A). A custom MATLAB script was used to quantify this intensity change as a function of distance and is shown in Figure 6C. Regardless of the coating condition, the Iba1 intensity increased initially and then declined to reach a background level further from the interface. Peak Iba1 intensity occurred at approximately 35.0 μm (3.5 ± 0.3), 45.0 μm (2.5 ± 0.3) and 25.0 μm (2.8 ± 0.3) for NC, PC-coated and PCD-coated electrodes, respectively. Statistically significant decreases in Iba1 intensity compared to the NC electrodes were observed for the PC-coated electrodes at distances of 15 μm, 25 μm, 35 μm ($p < 0.001$) and 85 μm ($p < 0.05$).

Vimentin immunoreactivity was relatively homogenous throughout the tissue indicating that the implanted electrode and chronic stimulation do not elicit a pronounced effect on vimentin-positive cells (including endothelial cells and macrophages) (Figure 7). Staining for the transmembrane cell surface glycoprotein L1 was performed, and increased L1 immunoreactivity was observed around the interface with background levels found further from this interface (Figure 7).

Finally, to determine the impact on neuronal cell death, the colocalization of NeuN and activated caspase-3 was determined (example images provided in Figure 8). Both PC-coated and PCD-coated electrodes were associated with a decrease in the percentage of neuronal cell death as assessed by the number of NeuN/caspase-3 positive cells versus NeuN positive cells when compared to the NC controls (Table 3).

4. Discussion

Peripheral nervous system sites like the DRG are potential locations for implanting long-term neural interfaces or neuroprosthetics. In this study, we have evaluated the cellular response to non-coated Pt/Ir electrodes as well as electrodes modified with conducting polymer in response to stimulation. Our results indicate that electrode performance and neuronal health are significantly improved in the presence of the PC and PCD surface modifications.

Lower impedance values were observed with the coatings *in vitro*. These differences were not observed *in vivo* for the electrodes that were not subjected to the stimulation paradigm. In this complex microenvironment, factors other than the coatings contribute to the measured impedance values and may mitigate the beneficial effects observed *in vitro*. Decreased impedance values were observed with the coatings at early (1-3 days; PCD versus NC) and middle (4-7 days; PC and PCD versus NC) time points *in vivo*; however, no

statistically significant differences were observed at later time points (8-10 days). The decreased impedance observed with the PCD coating suggests a beneficial effect of drug release as compared to the PC coating although the long-term implications of these effects are unclear. Extended studies (> 4 weeks) will be required to determine if the early benefits translate to an improved chronic electrode-tissue interface. While this *in vitro* and early chronic *in vivo* work demonstrates a proof-of-concept platform for drug-releasing stimulation electrodes, recent work suggests that the first 12 hours to 21 days post-implant may be the most dynamic and most useful for interventions aimed at promoting long-term function [10]; sustained dexamethasone release during this time period may be especially important. Furthermore, ultrasmall electrodes may be needed to extend early benefits to long-term performance [23, 24].

In peripheral tissues like the DRG, it is believed that immune cells invade following injury [53, 54] and some microglia/macrophages express Iba1. Using this marker as an indication of the inflammatory reaction, our results indicate that electrodes modified with conducting polymers have less of an inflammatory reaction as compared to unmodified electrodes. However, no significant differences in Iba1 intensity were observed when the PCD-coated electrodes were compared to the NC electrodes. This is similar to the results obtained with silicon neural probes with and without dexamethasone at 4 weeks post-implantation [52] and may be due to drug depletion or stabilization of the inflammatory response as previously proposed.

To assess the effects of localized dexamethasone release, PC-coated and PCD-coated electrodes were compared. No significant differences in the radius of the kill zone were observed although the total amount of neuronal cell death was lower with the PCD coating than with the PC coating (14.1% versus 19.7%). A similar result was obtained by Zhong and Bellamkonda in the brain; more NF160 staining was observed with dexamethasone-coated silicon neural probes at both 1 week and 4 weeks post implantation [52]. With respect to the inflammatory reaction, peak intensity of Iba1 occurred further from the implant site for the PC coating than for the PCD coating (45.0 μm versus 25.0 μm). Although there were areas of higher Iba1 intensity with dexamethasone, the PCD coating was associated with a smaller overall area of inflammation. This is consistent with studies demonstrating dexamethasone's ability to inhibit the immune response [16, 51, 52]. Although scarring would not be expected in this relatively short-term study, dexamethasone has also been shown to have inhibitory effects on this related process [16, 51, 52, 55]. Alternative drugs or combinations thereof may prove more effective in controlling the immune response and glial activation; certainly, combinatorial approaches are effective for promoting neurite outgrowth [56]. However, the results presented in this paper provide evidence that this platform can be used to load and release therapeutic agents *in vivo* in a controlled, localized fashion.

To ensure that the coatings were not intrinsically causing an unpredicted tissue reaction suppressed by the electrical stimulation, impedance values and the cellular response with and without stimulation were compared. With stimulation we observed a decrease in impedance with time as has been observed transiently by others [57]. Histologically speaking, this lower impedance was associated with significantly improved neuronal health. This study is the first to evaluate the performance of the PC and PCD coatings *in vivo*.

Although only 1-2 animals/coating were included for the no stimulation controls, we were able to ensure that a massive tissue response was not elicited by the coatings themselves.

In comparing coated versus uncoated electrodes, smaller kill zones were observed with the polymer coatings and the amount of neuronal cell death was less than half of that observed without coating. Similarly, the extent of inflammation was decreased when modified electrodes were compared with NC electrodes. Although the complex nature of the electrode-tissue interface makes simple cause-effect relationships difficult, the lower impedance electrodes (i.e., those with the conducting polymer coating) experience a lower voltage for the given stimulation paradigm. This reduced potential not only impacts electrical recording properties but should cause less tissue damage. The interplay between these factors and the time scale at which these interactions occur can be investigated further in subsequent studies that include multiple time points.

While our laboratory has previously investigated PPy/CNT/Dexamethasone and PEDOT/CNT, this study is the first report of the PEDOT/CNT/Dexamethasone coating. This novel coating combines the stability of PEDOT with the drug-loading capacity of CNTs to deliver an anti-inflammatory agent directly to the electrode-tissue interface. The stimulation protocol employed was modeled after those utilized for intracortical microstimulation of visual prosthetic devices [44] and for sensorimotor cortex stimulation [42] and differs from that used in prior studies [41]. While limiting the extent of tissue damage will remain the priority, stronger stimuli or thicker coatings to allow greater drug release or loading could be investigated. Despite the fact that charge-balanced paradigms are preferred for functional applications to prevent charge build-up, optimal drug release may need to be more negatively biased or administered at a lower frequency. Additionally, electrodes that more closely match the mechanical properties of the target tissue should minimize mismatch-associated damage caused by micro-motion and/or the foreign body response and must be considered as well.

Apoptosis, one type of programmed cell death, occurs following nervous system injury [58, 59] and can be triggered by a variety of insults that can lead to apoptotic cell death including those that impact cells away from the interface (i.e., cytokines, inflammation, excitotoxicity and free radical damage) [58, 60, 61]. Our coated electrodes appear to reduce this secondary mechanism of damage. Similarly, the smaller kill zone size observed with the coated electrodes indicates that these electrodes promote neuronal and axonal survival. These findings are consistent with previous work investigating dexamethasone release in which reduced neuronal loss was observed at 1 and 4 week time points [52].

For one implant in each coating condition, there was a compromised interface for which the location of the two electrodes could not be visualized. Rather, one large interface was observed (example images provided in the supplementary figures). This may be due to removal of the tissue with the electrode as a result of bent electrode tips. Another possible explanation for this variability in tissue reaction is the extent of injury to key vascular structures caused by the implant [62, 63]. For future applications, more accurate targeting to the nerve root would be valuable. In addition, the impact of these coatings on parameters like recording quality and signal drift could be evaluated.

In the current study, strong L1 staining was found around implanted electrodes. L1 has been shown to be up-regulated following nervous system injury both *in vitro* (reviewed in [64]) and *in vivo* [65, 66]. This up-regulation is thought to promote neural repair and regeneration. For example, in mouse models of Parkinson's disease and in spinal cord injury models L1 has been shown to improve cell survival [67, 68]. Increased L1 immunoreactivity with PC-coated and PCD-coated electrodes may indicate regeneration of injured neurons or axons near the implant site as L1 mediates peripheral myelin formation [69]. In cases in which a high degree of neurons are lost or degenerating, L1 expression may indicate compensatory sprouting from nearby healthy neurons. Further studies are required to better understand the roles of L1 particularly in the peripheral nervous system. At the present time, we suggest that L1 may be used as a robust marker of regenerative responses post-injury; it does not necessarily indicate functional recovery but activation of the injury/repair cascade.

This study is the first to report on the PC and PCD coatings in an *in vivo* model involving stimulation. It suggests that controlled and localized release of anti-inflammatory agents can minimize the overall area associated with the inflammatory response and maintain neuronal health when compared to NC electrodes. The high stability of PEDOT coupled with the drug-loading capacity of CNTs warrant additional testing and optimization to achieve long-term stability at the electrode-tissue interface.

Supplementary Material

Refer to Web version on PubMed Central for supplementary material.

Acknowledgments

The authors wish to thank Simon Watkins, Ph.D. and the Center for Biologic Imaging of the University of Pittsburgh for providing confocal training and assistance and Tyler Simpson for his help with microstimulator set-up and stimulation software/programming. Funding for this work was provided in part by the Department of Defense TATRC grant WB1XWH-07-1-0716 and the National Institutes of Health R01NS062019.

References

1. Richardson-Burns SM, Hendricks JL, Martin DC. Electrochemical polymerization of conducting polymers in living neural tissue. J Neural Eng. 2007; 4(2):L6–L13. [PubMed: 17409471]
2. Gaunt RA, Hokanson JA, Weber DJ. Microstimulation of primary afferent neurons in the L7 dorsal root ganglia using multielectrode arrays in anesthetized cats: thresholds and recruitment properties. J Neural Eng. 2009; 6(5):055009. [PubMed: 19721181]
3. Vallbo AB. Sensations evoked from the glabrous skin of the human hand by electrical stimulation of unitary mechanosensitive afferents. Brain Res. 1981; 215(1-2):359–63. [PubMed: 7260595]
4. Ochoa J, Torebjork E. Sensations evoked by intraneural microstimulation of single mechanoreceptor units innervating the human hand. J Physiol. 1983; 342:633–54. [PubMed: 6631752]
5. Macefield G, Gandevia SC, Burke D. Perceptual responses to microstimulation of single afferents innervating joints, muscles and skin of the human hand. J Physiol. 1990; 429:113–29. [PubMed: 2148951]
6. Ohara S, Weiss N, Lenz FA. Microstimulation in the region of the human thalamic principal somatic sensory nucleus evokes sensations like those of mechanical stimulation and movement. J Neurophysiol. 2004; 91(2):736–45. [PubMed: 14573561]
7. Cogan SF. Neural stimulation and recording electrodes. Annu Rev Biomed Eng. 2008; 10:275–309. [PubMed: 18429704]

8. McConnell GC, et al. Implanted neural electrodes cause chronic, local inflammation that is correlated with local neurodegeneration. J Neural Eng. 2009; 6(5):056003. [PubMed: 19700815]
9. Biran R, Martin DC, Tresco PA. Neuronal cell loss accompanies the brain tissue response to chronically implanted silicon microelectrode arrays. Exp Neurol. 2005; 195(1):115–26. [PubMed: 16045910]
10. Prasad A, et al. Comprehensive characterization and failure modes of tungsten microwire arrays in chronic neural implants. J Neural Eng. 2012; 9(5):056015. [PubMed: 23010756]
11. Johnson MD, Otto KJ, Kipke DR. Repeated voltage biasing improves unit recordings by reducing resistive tissue impedances. IEEE Trans Neural Syst Rehabil Eng. 2005; 13(2):160–5. [PubMed: 16003894]
12. Vetter RJ, et al. Chronic neural recording using silicon-substrate microelectrode arrays implanted in cerebral cortex. IEEE Trans Biomed Eng. 2004; 51(6):896–904. [PubMed: 15188856]
13. Rathnasingham R, et al. Characterization of implantable microfabricated fluid delivery devices. IEEE Trans Biomed Eng. 2004; 51(1):138–45. [PubMed: 14723503]
14. Zhong Y, Bellamkonda RV. Controlled release of anti-inflammatory agent alpha- MSH from neural implants. J Control Release. 2005; 106(3):309–18. [PubMed: 15978692]
15. Williams JC, et al. Multi-site incorporation of bioactive matrices into MEMS-based neural probes. J Neural Eng. 2005; 2(4):L23–8. [PubMed: 16317225]
16. Spataro L, et al. Dexamethasone treatment reduces astroglia responses to inserted neuroprosthetic devices in rat neocortex. Exp Neurol. 2005; 194(2):289–300. [PubMed: 16022859]
17. Jain A, et al. In situ gelling hydrogels for conformal repair of spinal cord defects, and local delivery of BDNF after spinal cord injury. Biomaterials. 2006; 27(3):497–504. [PubMed: 16099038]
18. Ware T, et al. Fabrication of Responsive, Softening Neural Interfaces. Advanced Functional Materials. 2012 n/a-n/a.
19. Capadona JR, et al. Stimuli-responsive polymer nanocomposites inspired by the sea cucumber dermis. Science. 2008; 319(5868):1370–4. [PubMed: 18323449]
20. Harris JP, et al. Mechanically adaptive intracortical implants improve the proximity of neuronal cell bodies. J Neural Eng. 2011; 8(6):066011. [PubMed: 22049097]
21. Harris JP, et al. In vivo deployment of mechanically adaptive nanocomposites for intracortical microelectrodes. J Neural Eng. 2011; 8(4):046010. [PubMed: 21654037]
22. Kozai TD, Kipke DR. Insertion shuttle with carboxyl terminated self-assembled monolayer coatings for implanting flexible polymer neural probes in the brain. J Neurosci Methods. 2009; 184(2):199–205. [PubMed: 19666051]
23. Gilgunn PJ, et al. An ultra-compliant, scalable neural probe with molded biodissolvable delivery vehicle. IEEE 25th International Conference on Micro Electro Mechanical Systems (MEMS). 2012:56–9.
24. Kozai TD, et al. Ultrasmall implantable composite microelectrodes with bioactive surfaces for chronic neural interfaces. Nat Mater. 2012; 11(12):1065–73. [PubMed: 23142839]
25. Guitchounts G, et al. A carbon-fiber electrode array for long-term neural recording. J Neural Eng. 2013; 10(4):046016. [PubMed: 23860226]
26. Wilks SJ, et al. Poly(3,4-ethylenedioxythiophene) as a Micro-Neural Interface Material for Electrostimulation. Front Neuroeng. 2009; 2:7. [PubMed: 19543541]
27. Abidian MR, Kim DH, Martin DC. Conducting-Polymer Nanotubes for Controlled Drug Release. Adv Mater. 2006; 18(4):405–409. [PubMed: 21552389]
28. Cui XT, Zhou DD. Poly (3,4-ethylenedioxythiophene) for chronic neural stimulation. IEEE Trans Neural Syst Rehabil Eng. 2007; 15(4):502–8. [PubMed: 18198707]
29. Nyberg T, Shimada A, Torimitsu K. Ion conducting polymer microelectrodes for interfacing with neural networks. J Neurosci Methods. 2007; 160(1):16–25. [PubMed: 17000006]
30. Groenendaal L, Jonas F, Freitag D, Pielartzik H, Reynolds JR. Poly(3,4- ethylenedioxythiophene) and Its Derivatives: Past, Present, and Future. Adv. Mater. 2000; 12(7):481–494.
31. Green RA, et al. Substrate dependent stability of conducting polymer coatings on medical electrodes. Biomaterials. 2012; 33(25):5875–86. [PubMed: 22656446]

32. Wadhwa R, Lagenaur CF, Cui XT. Electrochemically controlled release of dexamethasone from conducting polymer polypyrrole coated electrode. J Control Release. 2006; 110(3):531–41. [PubMed: 16360955]
33. Luo X, et al. Highly stable carbon nanotube doped poly(3,4-ethylenedioxythiophene) for chronic neural stimulation. Biomaterials. 2011; 32(24):5551–7. [PubMed: 21601278]
34. Blanchet GB, Fincher CR, Gao F. Polyaniline nanotube composites: A high- resolution printable conductor. Appl. Phys. Lett. 2003; 82(8):1290–1293.
35. Kilbride BE, Coleman JN, Fraysse J, Fournet P, Cadek M, Drury A, Hutzler S, Roth S, Blau WJ. Experimental observation of scaling laws for alternating current and direct current conductivity in polymer-carbon nanotube composite thin films. J. Appl. Phys. 2002; 92(7):4024–4031.
36. Dumortier H, et al. Functionalized carbon nanotubes are non-cytotoxic and preserve the functionality of primary immune cells. Nano Lett. 2006; 6(7):1522–8. [PubMed: 16834443]
37. Sayes CM, et al. Functionalization density dependence of single-walled carbon nanotubes cytotoxicity in vitro. Toxicol Lett. 2006; 161(2):135–42. [PubMed: 16229976]
38. Green RA, et al. Novel neural interface for implant electrodes: improving electroactivity of polypyrrole through MWNT incorporation. J Mater Sci Mater Med. 2008; 19(4):1625–9. [PubMed: 18214647]
39. Bianco A, Kostarelos K, Prato M. Applications of carbon nanotubes in drug delivery. Curr Opin Chem Biol. 2005; 9(6):674–9. [PubMed: 16233988]
40. Bhirde AA, et al. Targeted killing of cancer cells in vivo and in vitro with EGF- directed carbon nanotube-based drug delivery. ACS Nano. 2009; 3(2):307–16. [PubMed: 19236065]
41. Luo X, et al. Carbon nanotube nanoreservior for controlled release of anti- inflammatory dexamethasone. Biomaterials. 2011; 32(26):6316–23. [PubMed: 21636128]
42. McCreery D, Pikov V, Troyk PR. Neuronal loss due to prolonged controlled- current stimulation with chronically implanted microelectrodes in the cat cerebral cortex. J Neural Eng. 2010; 7(3): 036005. [PubMed: 20460692]
43. Bak M, et al. Visual sensations produced by intracortical microstimulation of the human occipital cortex. Med Biol Eng Comput. 1990; 28(3):257–9. [PubMed: 2377008]
44. Schmidt EM, et al. Feasibility of a visual prosthesis for the blind based on intracortical microstimulation of the visual cortex. Brain. 1996; 119(Pt 2):507–22. [PubMed: 8800945]
45. Merrill DR, Bikson M, Jefferys JG. Electrical stimulation of excitable tissue: design of efficacious and safe protocols. J Neurosci Methods. 2005; 141(2):171–98. [PubMed: 15661300]
46. Kolarcik CL, et al. In vivo effects of L1 coating on inflammation and neuronal health at the electrode-tissue interface in rat spinal cord and dorsal root ganglion. Acta Biomater. 2012; 8(10): 3561–75. [PubMed: 22750248]
47. Weber DJ, et al. Limb-state feedback from ensembles of simultaneously recorded dorsal root ganglion neurons. J Neural Eng. 2007; 4(3):S168–80. [PubMed: 17873416]
48. Zhou H, et al. Poly(3,4-ethylenedioxythiophene)/multiwall carbon nanotube composite coatings for improving the stability of microelectrodes in neural prostheses applications. Acta Biomater. 2013
49. Philibert J. Atom Movements: Diffusion and Mass Transport in Solids. 1991
50. Saltzman WM, Radomsky ML. Drugs released from polymers: diffusion and elimination in brain tissue. Chemical Engineering Science. 1991; 46(10):2429–2444.
51. Shain W, et al. Controlling cellular reactive responses around neural prosthetic devices using peripheral and local intervention strategies. IEEE Trans Neural Syst Rehabil Eng. 2003; 11(2): 186–8. [PubMed: 12899270]
52. Zhong Y, Bellamkonda RV. Dexamethasone-coated neural probes elicit attenuated inflammatory response and neuronal loss compared to uncoated neural probes. Brain Res. 2007; 1148:15–27. [PubMed: 17376408]
53. Bennett DL, et al. A distinct subgroup of small DRG cells express GDNF receptor components and GDNF is protective for these neurons after nerve injury. J Neurosci. 1998; 18(8):3059–72. [PubMed: 9526023]

54. Hu P, et al. Immune cell involvement in dorsal root ganglia and spinal cord after chronic constriction or transection of the rat sciatic nerve. Brain Behav Immun. 2007; 21(5):599–616. [PubMed: 17187959]

55. Jaquins-Gerstl A, et al. Effect of dexamethasone on gliosis, ischemia, and dopamine extraction during microdialysis sampling in brain tissue. Anal Chem. 2011; 83(20):7662–7. [PubMed: 21859125]

56. Thompson BC, et al. Conducting polymers, dual neurotrophins and pulsed electrical stimulation--dramatic effects on neurite outgrowth. J Control Release. 2010; 141(2):161–7. [PubMed: 19788902]

57. Hemm S, et al. Evolution of brain impedance in dystonic patients treated by GPI electrical stimulation. Neuromodulation. 2004; 7(2):67–75. [PubMed: 22151186]

58. Dumont RJ, et al. Acute spinal cord injury, part I: pathophysiologic mechanisms. Clin Neuropharmacol. 2001; 24(5):254–64. [PubMed: 11586110]

59. Paterniti I, et al. Treatment with green tea extract attenuates secondary inflammatory response in an experimental model of spinal cord trauma. Naunyn Schmiedebergs Arch Pharmacol. 2009; 380(2):179–92. [PubMed: 19337722]

60. Amemiya S, et al. Anti-apoptotic and neuroprotective effects of edaravone following transient focal ischemia in rats. Eur J Pharmacol. 2005; 516(2):125–30. [PubMed: 15921675]

61. Oyinbo CA. Secondary injury mechanisms in traumatic spinal cord injury: a nugget of this multiply cascade. Acta Neurobiol Exp (Wars). 2011; 71(2):281–99. [PubMed: 21731081]

62. Kozai TD, et al. Reduction of neurovascular damage resulting from microelectrode insertion into the cerebral cortex using in vivo two-photon mapping. J Neural Eng. 2010; 7(4):046011. [PubMed: 20644246]

63. Petterson CA, Olsson Y. Blood supply of spinal nerve roots. An experimental study in the rat. Acta Neuropathol. 1989; 78(5):455–61. [PubMed: 2816296]

64. Irintchev A, Schachner M. The Injured and Regenerating Nervous System: Immunoglobulin Superfamily Members as Key Players. Neuroscientist. 2011

65. Becker CG, et al. L1.1 is involved in spinal cord regeneration in adult zebrafish. J Neurosci. 2004; 24(36):7837–42. [PubMed: 15356195]

66. Becker T, et al. Differences in the regenerative response of neuronal cell populations and indications for plasticity in intraspinal neurons after spinal cord transection in adult zebrafish. Mol Cell Neurosci. 2005; 30(2):265–78. [PubMed: 16098761]

67. Chen J, et al. Cell adhesion molecule l1-transfected embryonic stem cells with enhanced survival support regrowth of corticospinal tract axons in mice after spinal cord injury. J Neurotrauma. 2005; 22(8):896–906. [PubMed: 16083356]

68. Cui YF, et al. Embryonic stem cell-derived L1 overexpressing neural aggregates enhance recovery in Parkinsonian mice. Brain. 2010; 133(Pt 1):189–204. [PubMed: 19995872]

69. Takeda Y, et al. The roles of cell adhesion molecules on the formation of peripheral myelin. Keio J Med. 2001; 50(4):240–8. [PubMed: 11806501]

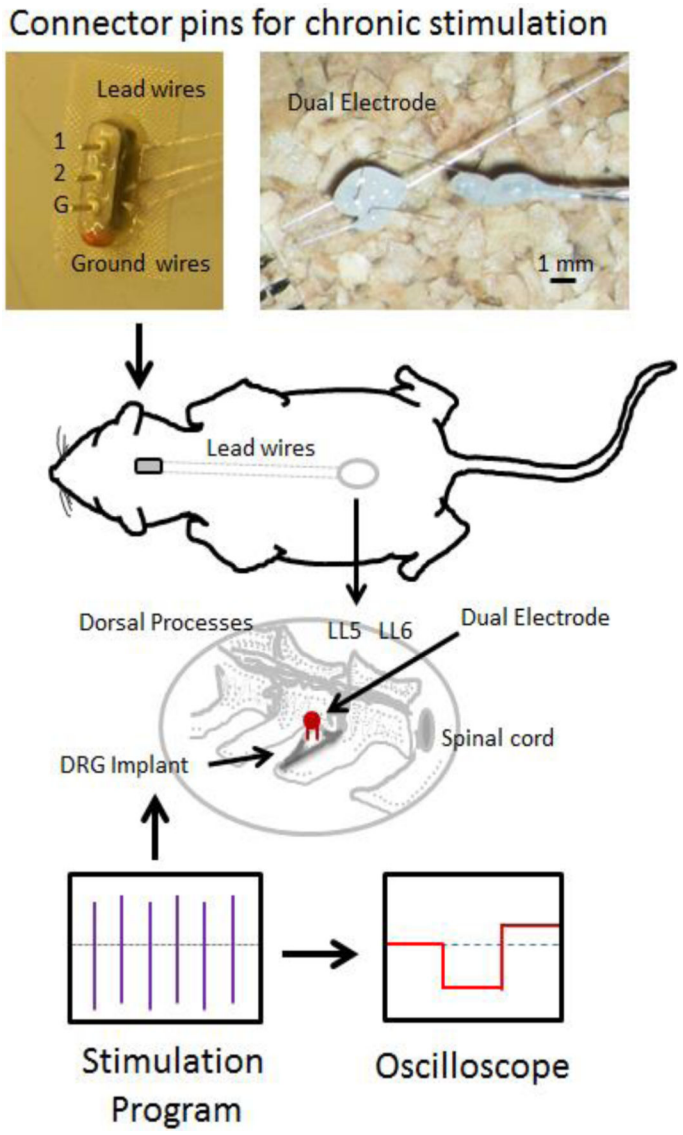

Figure 1.

Diagrammatic overview of the stimulation surgery. Dual electrodes were implanted into the DRG at L5 or L6. Lead wires ran from the electrodes up the back of the animal to an adaptor affixed to the skull. This head fixture allowed for repeated stimulation and included ground, electrode 1 (1) and electrode 2 (2) connections. Animals were subjected to 10 days of 400 μs pulses at 20 μAmps at 200 Hz for 1 hour/day and the stimulation paradigm monitored with an oscilloscope.

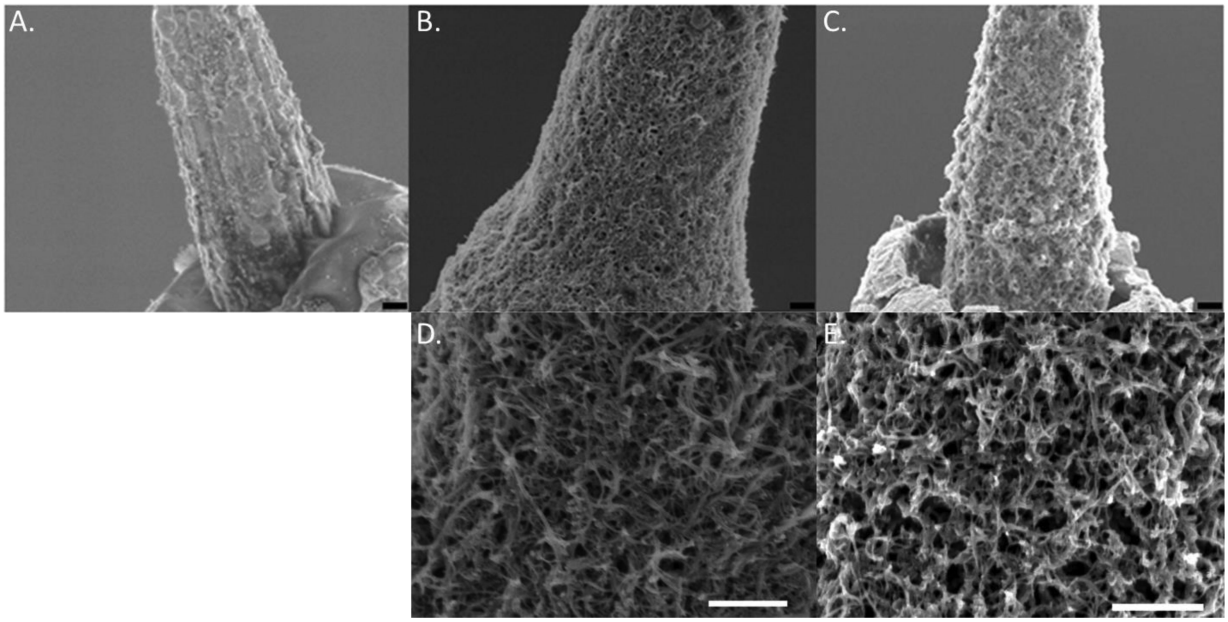

Figure 2.
Electrode coatings. Scanning electron micrograph (SEM) images of NC (A), PC (B, D) and PCD (C, E) electrodes. Scale bars represent 1 μm.

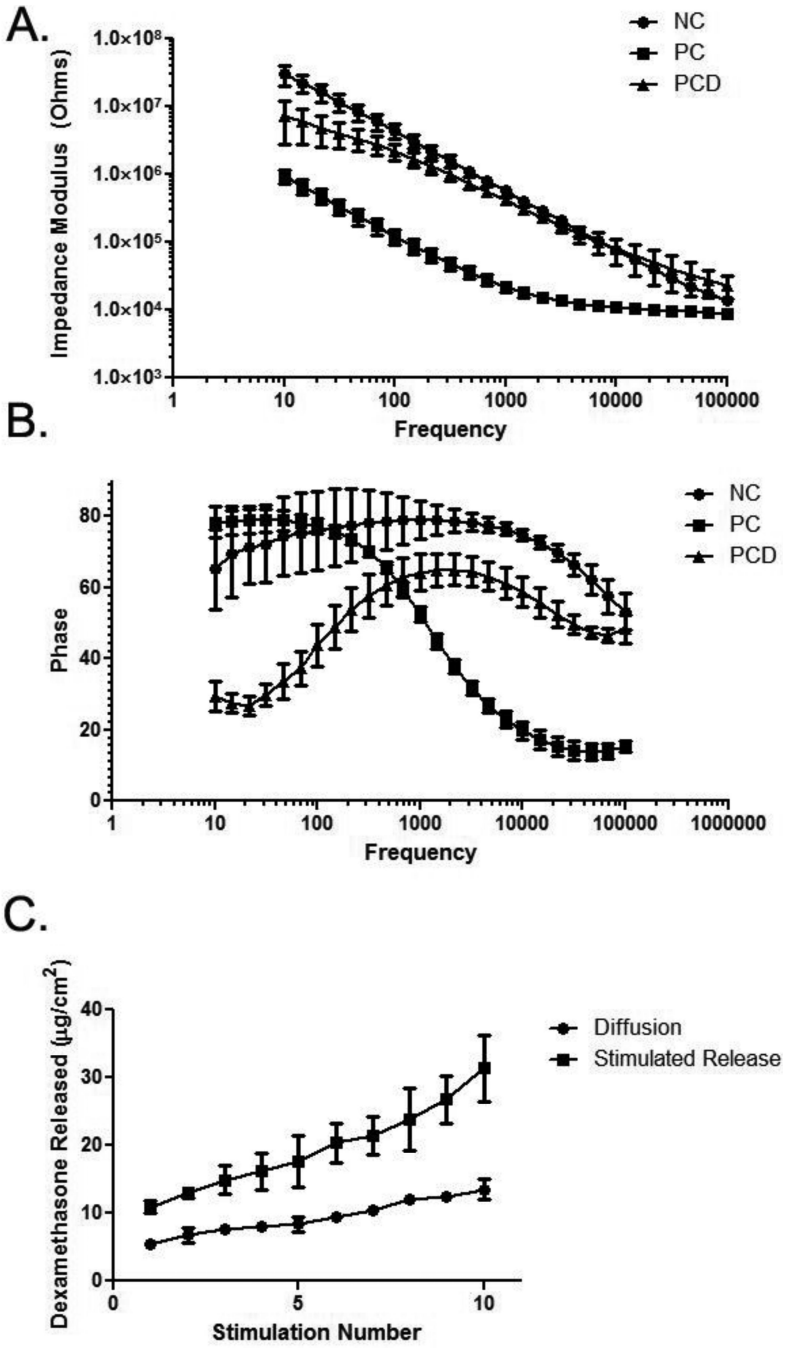

Figure 3.

In vitro impedance spectroscopy for NC, PC and PCD conditions. **A**: Bode plots. The lowest Z values were observed with the PC coating (solid squares) and incorporation of dexamethasone resulted in an impedance spectrum for the PCD coating (solid triangles) more similar to that observed with NC (solid circles). **B**: Phase plot indicating the different electrode-electrolyte interface behaviors for NC (solid circles), PC (solid squares) and PCD (solid triangles) coatings. Each plot includes data from $n = 3$ replicates, and error bars represent SD. **C**: Summed *in vitro* dexamethasone release. Over the ten stimulations applied

over the course of the *in vivo* study, dexamethasone was released with electrical stimulation (solid squares). Electrical stimulation triggered significantly more ($p < 0.0001$) drug release than that observed with passive diffusion (solid circles).

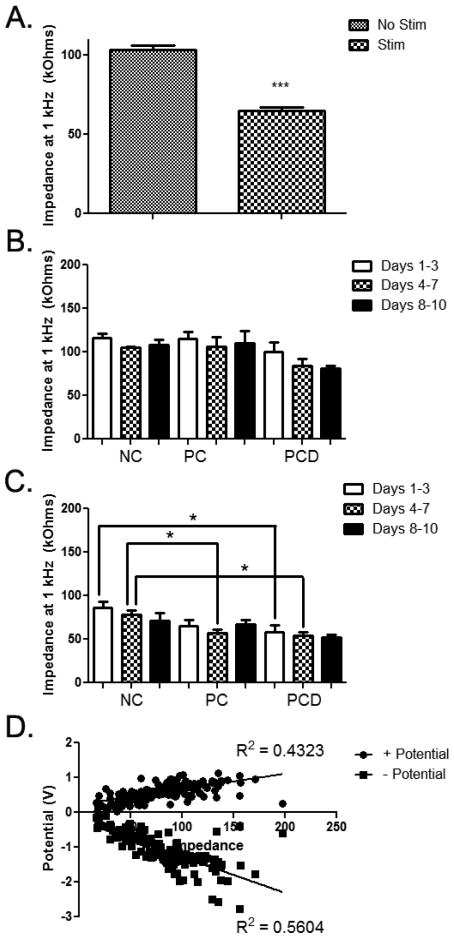

Figure 4.

In vivo electrode impedance (Z) at 1 kHz. **A**: With stimulation, there was a significant decrease in Z at 1 kHz when all coating conditions were combined. Error bars represent SEM. **B**: Impedance values at 1 kHz were grouped based on coating condition and time point in the study. No significant differences were observed across coatings and time points for electrodes that were not subjected to stimulation. Error bars represent SEM. **C**: Impedance values at 1 kHz were grouped based on coating condition and day of stimulation. Statistically significant decreases in Z were observed with the PC coating (4-7 days) and with the PCD coating (1-3 and 4-7 days) when compared to NC controls. Error bars represent SEM. **D**: Correlation between impedance and + potential and – potential. *p < 0.05: ***p < 0.001

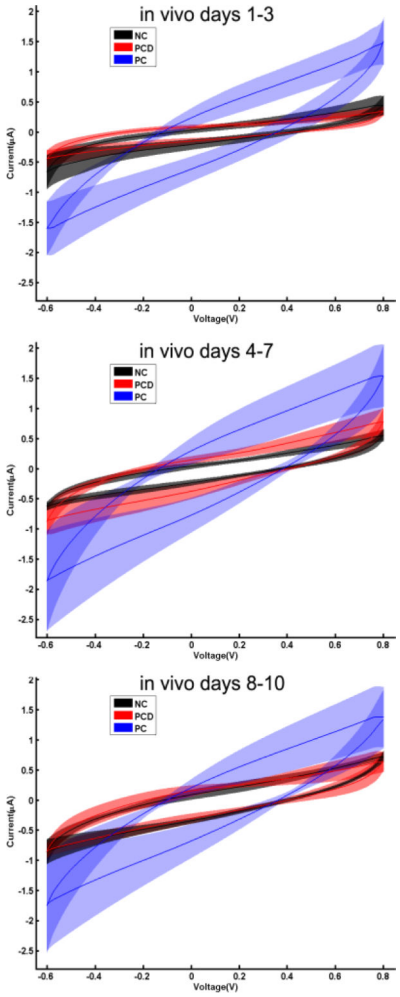

Figure 5.

Electrical characteristics of implanted electrodes. Cyclic voltammograms from each of the three electrode coatings for 1-3 (top), 4-7 (middle) and 8-10 (bottom) days *in vivo* are provided. The CVs from representative electrodes from NC (black), PC-coated (blue) and PCD-coated (red) were averaged and the mean shown as a solid line. The shaded area represents the SD.

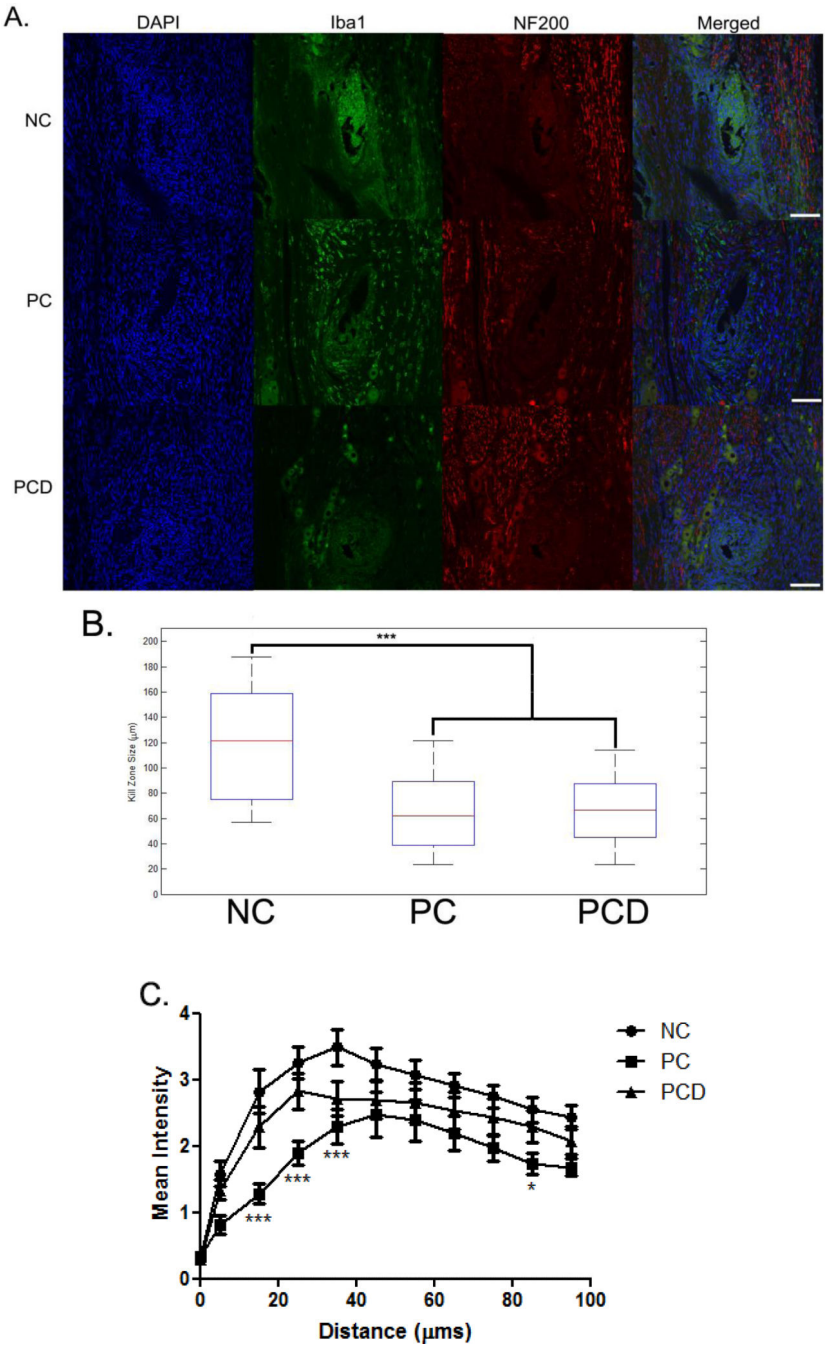

Figure 6.

NF-200 and Iba-1 expression in the DRG after stimulation. Immunofluorescence images of rat DRG stained for NF200 (red) and Iba1 (green). NF200 staining was lacking in the area immediately surrounding the implant site and differences assessed by measuring the size of the area void of this staining. Iba1-positive cells were localized around the implant site and this increased immunoreactivity quantified and compared. **A**: Representative images from each of the coating conditions after stimulation are provided. **B**: Kill zone size was compared by coating condition, and significant decreases were observed for coated

electrodes when compared to uncoated electrodes. **C**: Iba1 staining intensity as a function of distance from the electrode-tissue interface. Background staining was defined using corners of the analyzed image. Threshold values based on the background staining for each image were established, and Iba1 staining above this threshold measured as a function of distance from the implant site. The median intensity values were calculated in 10 μm bins and reported ± SEM. Scale bars represent 100 μm. *$p < 0.05$; ***$p < 0.001$

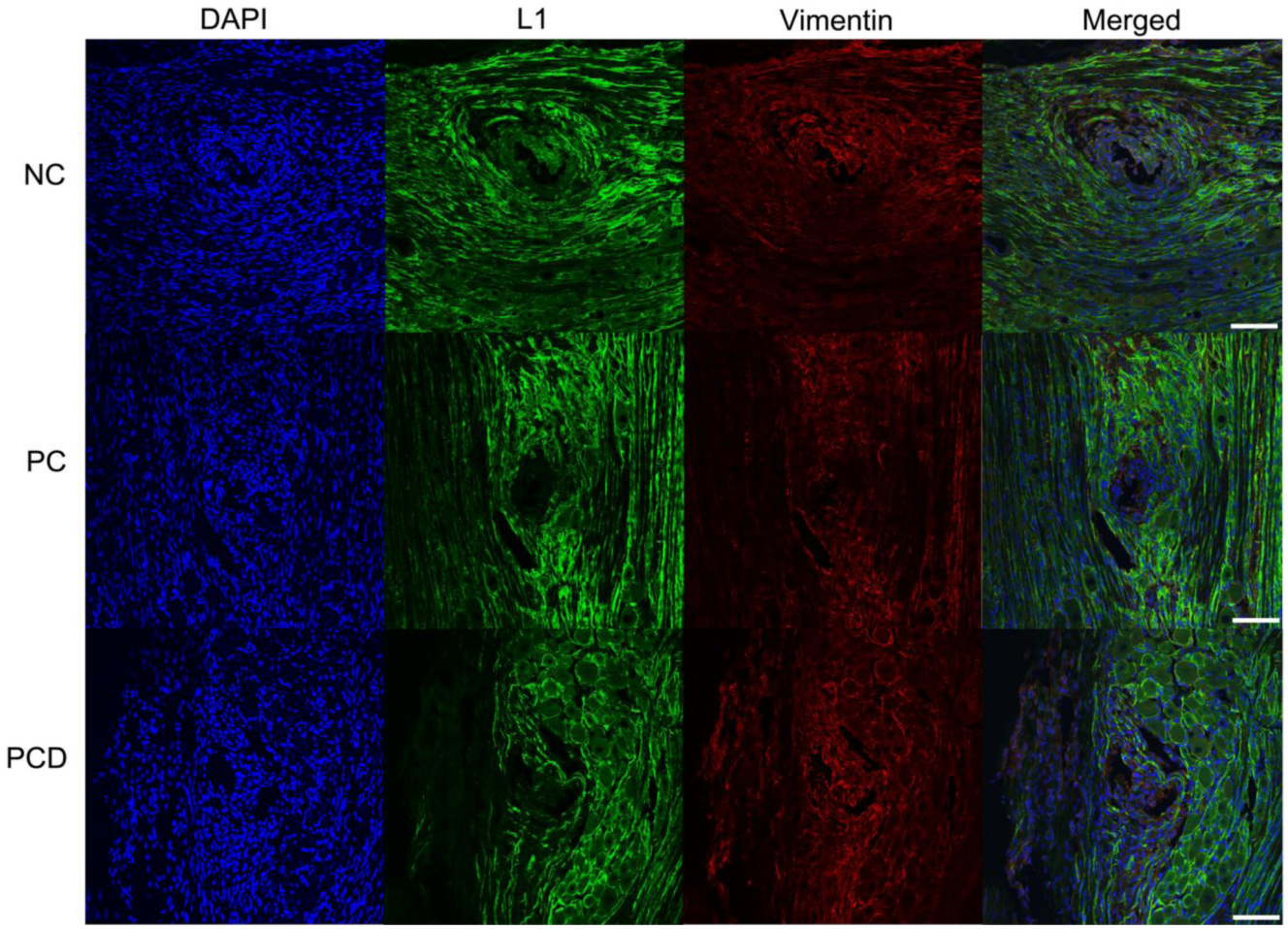

Figure 7.

L1 and vimentin expression in the DRG after stimulation. Immunofluorescence images of rat DRG stained for L1 (green) and vimentin (red) following implant of NC, PC and PCD neural probes. L1 staining was found around the implant site and associated with Schwann cells/peripheral myelin. Vimentin staining was relatively evenly distributed with some colocalization with L1. Representative images from each coating condition after stimulation. Scale bars represent 100 μm.

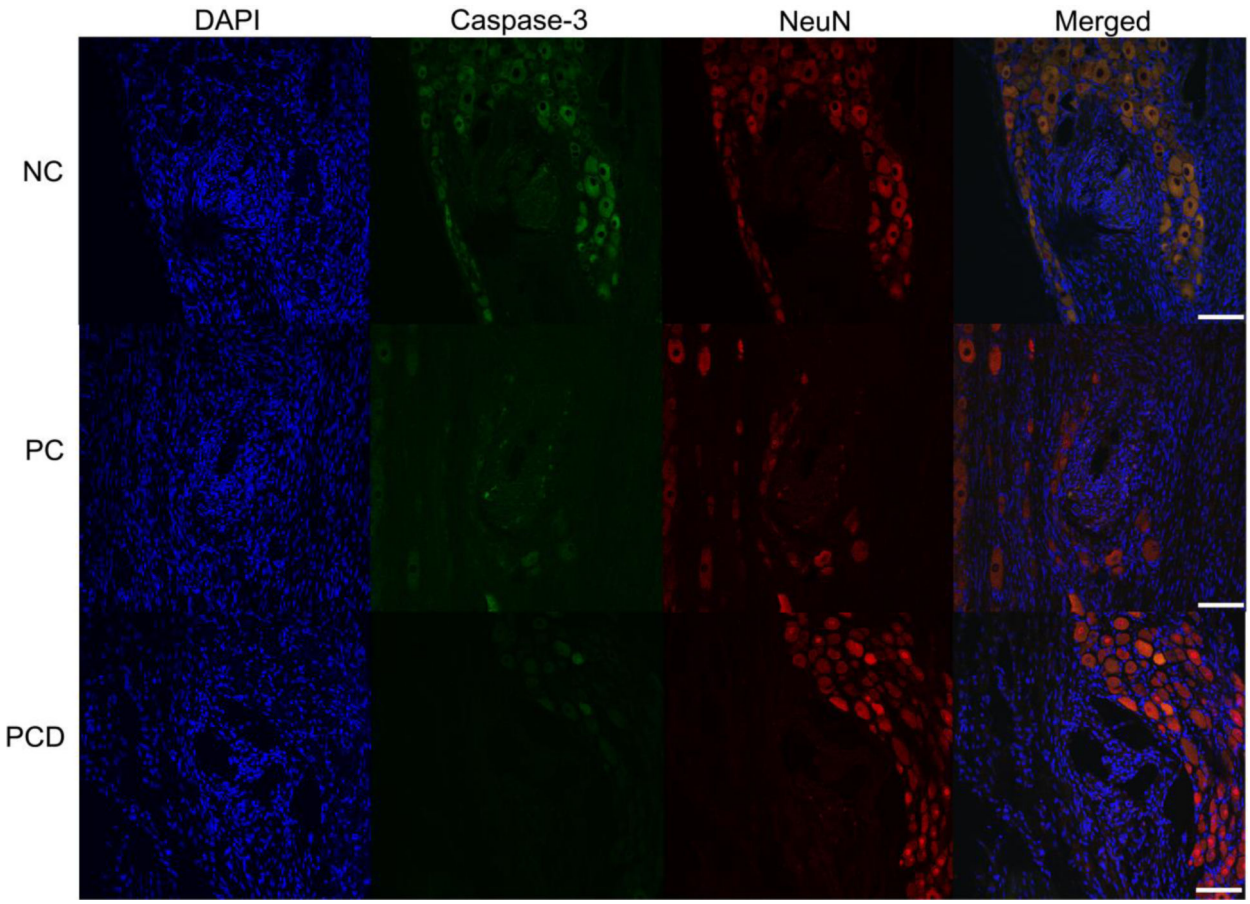

Figure 8.

Colocalization of NeuN and activated caspase-3 in the DRG. Immunofluorescence images were used to determine the degree of co-localization between NeuN (red) and cleaved caspase-3 (green) and representative images provided. The number of NeuN/caspase-3 positive cells was quantified and reported as a percentage of the total number of NeuN positive cells. Representative images are provided from each of the three coating conditions. Scale bars represent 100 μm.

Table 1

Animals in each treatment group

Coating Condition	Stimulation (Y/N)	Number of Electrode Shanks Evaluated
NC	N	3
	Y	6
PC	N	2
	Y	6
PCD	N	2
	Y	6

Table 2

Antibodies used for histological characterization

Antibody	Specificity
NF200	Mature axons
Iba1	Microglia/macrophages
L1	Neural cell adhesion molecule
Vimentin	Immature and reactive astrocytes, microglia, endothelial cells, fibroblasts
NeuN	Neuronal nuclei
Caspase-3	Cleaved (activated) caspase-3

Table 3

NeuN/Caspase-3 colocalization with stimulation

Coating Condition	Percentage of NeuN/Caspase-3 Positive Cells
NC	51.9% (204 of 393)
PC	19.7% (27 of 137)
PCD	14.1% (22 of 156)